Title
Assessing the diurnal cycle of precipitation in a multi-scale climate model

Journal
Journal of Advances in Modeling Earth Systems, 1(4)

ISSN
1942-2466

Authors
Pritchard, Michael S
Somerville, Richard C. J

Publication Date
2009-10-13

DOI
10.3894/JAMES.2009.1.12

J. Adv. Model. Earth Syst., **Vol. 1**, Art. #12, 16 pp.

Assessing the Diurnal Cycle of Precipitation in a Multi-Scale Climate Model

Michael S. Pritchard and Richard C. J. Somerville

Scripps Institution of Oceanography, University of California San Diego, La Jolla, CA

Manuscript submitted 17 November 2008; in final form 13 August 2009

A promising result that has emerged from the new Multi-scale Modeling Framework (MMF) approach to atmospheric modeling is a global improvement in the daily timing of peak precipitation over the continents, which is suggestive of improved moist dynamics at diurnal timescales overall. We scrutinize the simulated seasonal composite diurnal cycle of precipitation in an MMF developed by the Center for Multiscale Modeling of Atmospheric Processes (CMMAP) using a comprehensive suite of diurnal cycle diagnostics including traditional harmonic analysis, and non-traditional diagnostics such as the broadness of the peak precipitation in the mean summer day, reduced dimension transect analysis, and animations of the full spatial and temporal variability of the composite mean summer day. Precipitation in the MMF is evaluated against multi-satellite merged satellite data and a control simulation with a climate model that employs conventional cloud and boundary layer parameterizations. Our analysis highlights several improved features of the diurnal cycle of precipitation in the multi-scale climate model: It is less sinusoidal over the most energetic diurnal rainfall regimes, more horizontally inhomogeneous within continents and oceans, and more faithful to observed structural transitions in the composite diurnal cycle chronology straddling coastlines than the conventional climate model. A regional focus on North America links a seasonal summer dry bias over the continental United States in the CMMAP MMF at T42 resolution to its inability to capture diurnally propagating precipitation signals associated with organized convection in the lee of the Rockies. The chronology of precipitation events elsewhere in the vicinity of North America is improved in the MMF, especially over sea breeze circulation regions along the eastern seaboard and the Gulf of Mexico, as well as over the entirety of the Gulf Stream. Comparison of the convective heating and moistening suggests that improvements in the MMF coastal ocean diurnal rainfall may be a result of a local moist dynamical response to the improved representation of energetic diurnal forcing over adjacent land.

DOI:10.3894/JAMES.2009.1.12

1. Introduction

1.1. Multi-scale Modeling Frameworks (MMFs)

MMFs represent a new approach to climate modeling that has emerged in recent years as a potential workaround to the age-old "cloud climate" dilemma (Randall et al. 2003). The problem is that cloud processes cover an immense range of spatial and temporal scales - from the microcosm of droplet growth microphysics to the large scale geophysical fluid dynamics governing storm systems of continental scale. No supercomputer is powerful enough to produce decadal or centennial-scale climate projections while simulating the physics of the entire range of scales, so processes below a certain truncation spatial scale (usually about 100 km) are instead represented with simple models called parameterizations in conventional climate models. MMFs break tradition with this approach, as originated by Grabowski and Smolarkiewicz (1999), by employing a host coarse-resolution global climate model that houses in each of its grid columns a small subdomain of high resolution cloud-resolving model (CRM) columns representing a small fraction of the total area of the host grid column. Statistics harvested from an idealized nested, non-hydrostatic, "cloud system"-resolving integration are assumed to represent the entire area, and replace the conventional parameterizations for unresolved cloud fluxes of heat and moisture, and boundary layer processes. This approach is sometimes referred to as "super-parameterization".

MMFs are more than two orders of magnitude more expensive to run than conventional global climate models but exhibit considerably more efficient parallel scalability (Grabowski and Smolarkiewicz (1999); Khairoutdinov et al. 2005), making climate scale integrations realizable within

To whom correspondence should be addressed.
Michael S. Pritchard, Scripps Graduate Department, Mail Code 0224, 9500 Gilman Drive, La Jolla, CA, 92093-0224. COURIER: 8810 Shellback Way, Nierenberg Hall Rm. 425, La Jolla CA 92037
mikepritchard@ucsd.edu

reasonable timeframes on the order of a thousand processors. They are intended for use as an interim tool to begin probing the nature of multi-scale interactions between fast/regional processes and slow/global climate evolution, for the decades before global cloud resolving simulations become affordable.

1.2. The diurnal cycle

Modern global climate models (GCMs) notoriously underperform when it comes to reproducing the sort of diurnal (24 hour) rainfall oscillations that are observed in nature (e.g. Collier and Bowman 2004). This is a problem for GCM climate projections, since biases in hydrologic variability at these short timescales indicate a disconnect between the physical drivers of convection in nature versus models; a warning sign that multi-scale physical relationships resulting in rainfall variability on longer timescales could also be distorted. The culprit is almost certainly imperfect cloud parameterizations - according to the latest synthesis report by the Intergovernmental Panel on Climate Change, the representation of unresolved cloud processes remains one of the largest sources of uncertainty in climate prediction.

Traditionally, a global view of diurnal variability is obtained by constructing spatial maps of some scalar metric that describes the time evolution of the climatological composite summer day time series (transformed to Local Solar Time, LST). There are many conceivable scalar descriptors of a composite day's time evolution; the most commonly scrutinized are the phase and amplitude of the least-squares-fitted 24-hour (S1; diurnal) and 12-hour (S2; semi-diurnal) harmonics (e.g. Chang et al. (1995), Dai (2001), Collier and Bowman (2004), Dai et al. (2004)) and the (unfitted) local time of peak precipitation. Less commonly employed, but important and complementary diagnostics of the composite diurnal cycle include the unfitted broadness of the daily maximum and reduced transect analysis (e.g. Carbone and Tuttle 2008), the precipitation range, and the amplitudes of leading empirical orthogonal functions (e.g. Kikuchi and Wang 2008). For regions in which the diurnal cycle is strongly tied to non-local forcing mechanisms, it is better to use an objective time coordinate (i.e. universal time coordinate, UTC) in order to visualize diurnally propagating signals.

Many traditional diagnostics of the diurnal rainfall cycle have previously been explored in MMFs and the results have been promising. Khairoutdinov et al. (2005) showed an improvement (relative to a conventional GCM) in the simulated local time of peak precipitation over continents in the SP-CAM (Super-Parameterized Community Atmosphere Model) MMF. This improvement in diurnal peak rainfall timing has also been documented in an independent MMF framework developed at NASA Goddard (Tao et al., 2009). Khairoutdinov et al. (2008) further demonstrated realistic relationships in SP-CAM between the diurnal variability of several stratocumulus properties (cloud liquid water, longwave cooling, vertical velocity variance, inversion height and sub-cloud vertical velocity skewness) for a single model grid point in the northeastern subtropical Pacific. DeMott et al. (2007) evaluated the simulated composite diurnal cycle of rainfall, convective available potential energy, convective inhibition, buoyancy and planetary boundary layer height, in three regional subdomains where nearby data from intense observing periods were available. Zhang et al. (2008) analyzed the amplitude and phase of the best-fit 24-hour harmonic of the July and January composite days' precipitation for the entire tropics from a 4-year SP-CAM simulation; they identified a weak bias in the 24-hour mode's precipitation amplitude during July over land, and an overall tendency for too much amplitude in the fitted 24-hour harmonic over the oceans, but otherwise reasonable agreement in the actual simulated precipitation in SP-CAM. Zhang et al. (2008) also used SP-CAM cloud water distributions harvested from the nested cloud-resolving subdomain scale as input to radiative transfer code, in order to emulate and evaluate the diurnal cycle of several operational proxies of precipitation and cloudiness that are routinely derived from space based measurements of infrared brightness temperature at two discrete frequency channels. They found significant deficiencies in the diurnal variability of these simulated top-of-the-atmosphere radiative and radar signals, and attributed them to an overall excess high cloud bias in SP-CAM.

In this study, we examine the simulated diurnal rainfall cycle in SP-CAM in much closer detail, extending the existing work to include several non-traditional metrics of composite diurnal precipitation that do not rely on curve fitting (diurnal peak broadness, reduced transect analysis, and regional animation) during DJF and JJA; results from empirical orthogonal function decomposition of the JJA diurnal rainfall cycle are separately reported in Pritchard and Somerville (2009). Our aim in adding these complementary vantage points to the existing body of diurnal MMF precipitation diagnostics is to clarify where (in order to better understand why) super-parameterized climate models exhibit improved regional moist convective circulations at diurnal timescales, at high levels of scrutiny. We compare the SP-CAM MMF against its counterpart GCM with conventional cumulus parameterization, and against a multi-satellite merged precipitation product.

1.3. Central United States diurnal variability

The central United States provides a telling example, and a challenging litmus test for any model of diurnal hydrologic variability. Over the central United States, the SP-CAM significantly underestimates JJA mean precipitation relative to both CAM and observations, despite showing considerable improvement in the statistics of light vs heavy rainfall (DeMott et al. 2007). The cause of the SP-CAM dry bias in this diurnally sensitive region have not been explored in detail, and are an additional focus of this study.

Observations indicate that the daily cycle of precipitation over the central United States is controlled by events upstream; convective initiation during the late afternoon over the sun-warmed Rockies self-organizes into mesoscale convective complexes (Carbone et al. 2002). Sustained by a favorable vertically sheared background wind environment, this organized convection is unusually long-lived, and drifts so far east that its precipitation dominates the diurnal cycle over the central United States, causing a late evening diurnal peak. This diurnal mechanism is primarily responsible for the climatological summer precipitation falling over the central United States (Carbone and Tuttle 2008). Conventional climate models have understandable difficulty capturing this phenomenon - at coarse resolution, the topographic heating features and the low-level dynamical environment that enable such MCC propagation are not resolved (Moncrieff and Liu 2006). In fact, DeMott et al. (2007) showed that although the Community Atmosphere Model appears to correctly simulate the seasonal scale precipitation over the central United States, it does so for the wrong reason- excess local evapotranspiration is produced in the land surface model's vegetative canopy as a result of mis-estimating the statistical distribution of light vs heavy rainfall.

2. Models, data and methods

2.1. The Super-Parameterized Community Atmosphere Model (SP-CAM)

The MMF used in this study is the SP-CAM v3.0, which is described in Khairoutdinov et al. (2005). Briefly, it is identical to the Community Atmosphere Model (CAM) v3.0 (Collins et al. 2006) except that the Zhang-McFarlane and Hack parameterizations, for deep and shallow sub-grid convection respectively, have been replaced with a nested integration of a two dimensional ($x - z$) realization of the cloud resolving model (CRM) described in Khairoutdinov and Randall (2003). The CRM solves the non-hydrostatic momentum equations of fluid dynamics subject to the anelastic approximation on an idealized 2D subdomain, using bulk microphysics that pertain to multiple categories of precipitating and non-precipitating prognostic water condensate variables, including ice, snow, liquid water, and graupel (Khairoutdinov and Randall 2003).

The two simulations analyzed are four month (MJJA, NDJF) integrations of the SP-CAM in which the host CAM horizontal resolution was approximately 2.8° latitude by 2.8° longitude (T42 spectral truncation). The first month is considered as spin-up, and only results from JJA and DJF are depicted in this paper. Within each CAM grid cell there were 32 nested CRM columns arranged zonally with a horizontal spacing of 4 km in a 128-km, laterally-periodic idealized subdomain, spanning less than half of the typical zonal extent of the host model grid points. At the large scale, SP-CAM was configured to run with a 15 minute timestep on 26 vertical levels, and the idealized embedded CRM was run with a 20 second timestep on vertical levels co-located with the 24 interior levels of CAM. In order to adequately resolve diurnal variability, model output was stored globally at three hourly increments, on both the host GCM and CRM scales. Corresponding single-summer control runs of CAM3.0 were also carried out for MJJA and NDJF as comparison.

2.2. Merged satellite precipitation product

As a baseline against which to compare simulated precipitation, we choose a rain gauge-scaled, multi-satellite, gridded 3-hourly, high resolution (0.25° by 0.25°) precipitation product called TRMM 3B42; this product is a best estimate that combines high quality microwave radiometer and precipitation radar data from the Tropical Rainfall Measuring Mission (TRMM) satellite with complementary but lower quality (but more abundant) infrared and microwave radiometer measurements from other platforms (see Huffman et al. 2007 for details). Of course, it would be more philosophically appealing to use as a ground truth only such raw, direct observations of precipitation as are available from dense networks of rain gauges, or perhaps from TRMM's precipitation radar alone. But the sampling biases that would be incurred by this strategy - in the case of the TRMM radar as a result of its narrow swath width (Hirose et al. 2008), and in the case of gauge data from inhomogeneities in the spatial distribution of weather stations - would unnecessarily complicate a large-scale analyses of the diurnal cycle. Since the climatological composite JJA diurnal cycle of precipitation in 3B42 has been well-studied and appears to be in good agreement with independent precipitation products and surface data (Dai et al. 2007), its practical advantages for the purpose of model comparison and evaluation are compelling.

2.3. Analysis methodology

Figure 1 contrasts the well documented seasonal scale biases in the JJA and DJF precipitation rates in the SP-CAM and CAM, showing that tropical seasonal precipitation biases are worse in both models (and especially the SP-CAM) during JJA than in DJF. During JJA, CAM exhibits the notorious ''double ITCZ (Intertropical Convergence Zone)'' problem, as well as excessive JJA orographic precipitation in the Indian Monsoon region. In the SP-CAM, the JJA double ITCZ problem is mitigated but the excessive monsoonal rainfall problem is exacerbated and a new tropical bias arises, known as the ''Great Wet Spot'', i.e. far too much simulated JJA precipitation in the Western Pacific (Luo and Stephens 2006; Khairoutdinov et al. 2005). During DJF, both models are in better agreement with the observed seasonal precipitation in the tropics, as evidenced by the RMS difference and pattern correlation values in Figure 1.

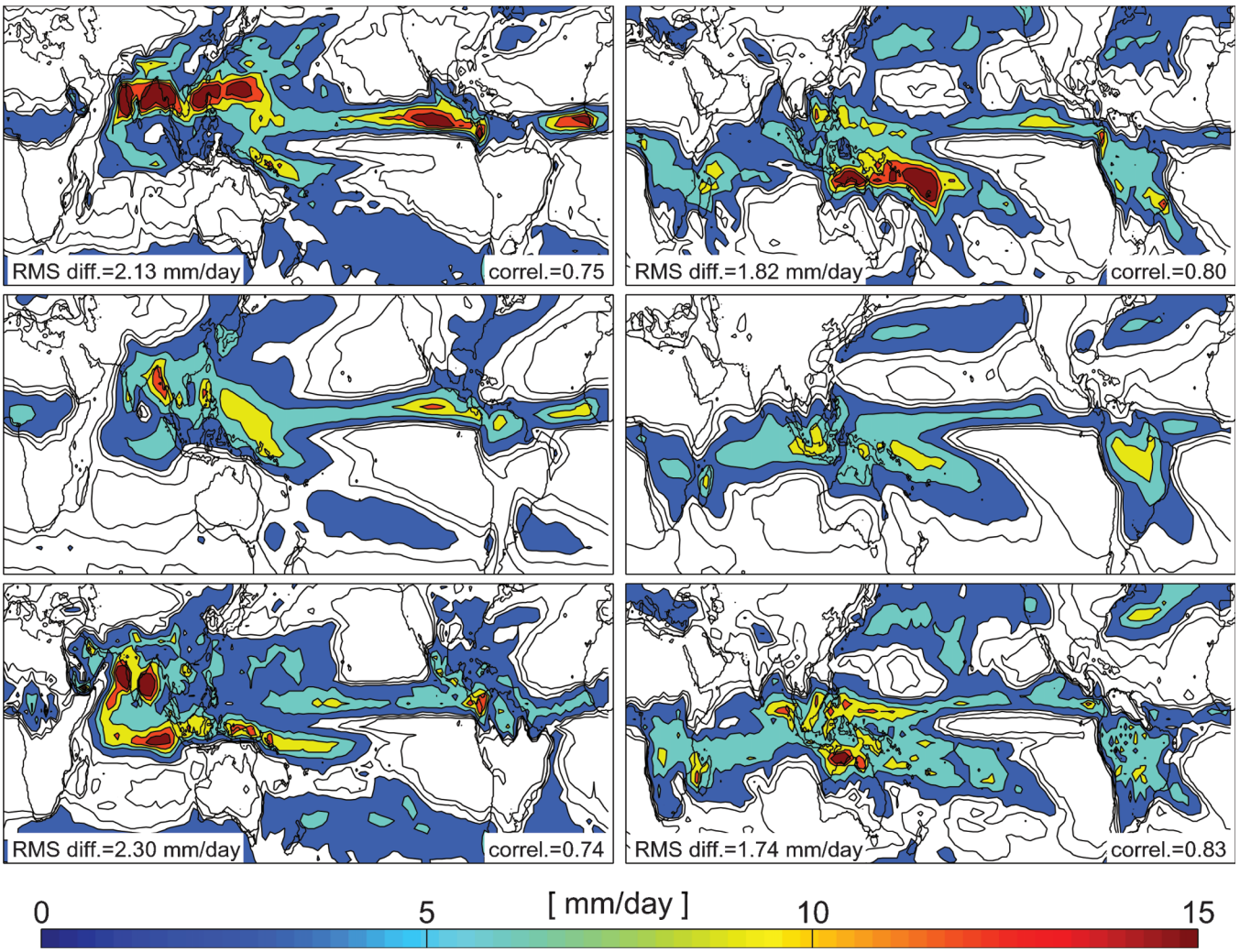

Figure 1. JJA (left) and DJF (right) precipitation for (top) three month simulation of SP-CAM, compared to (middle) 7 years of a merged multi-satellite, multi-instrument observational product (TRMM 3B42) and (bottom) CAM3.0. The contouring interval is 1 mm/day for precipitation rates below 3 mm/day (unshaded contours) and 3 mm/day for precipitation rates greater than or equal to 3 mm/day (shaded contours). Root-mean-squared difference and pattern correlation coefficient relative to the observations are shown for the two models.

This has consequences for the design of our analysis of simulated diurnal variability. Given the fact that the tropical diurnal cycle amplitude is fairly strong and seasonally invariant, the seasonality of model biases described above suggests DJF is a more appropriate season to study simulated diurnal variability than JJA, at least in the tropics. For the extratropics, diurnal variability is weaker and the greater diurnal signal-to-noise ratio afforded by more summer solar forcing and less baroclinicity and storm activity make JJA a better choice to study the simulated interior and coastal diurnal circulations of the northern hemisphere continents.

To gain a comprehensive view of the diurnal cycle of precipitation in model output and satellite observations, we apply a suite of complementary diurnal cycle diagnostics. All have as their starting point a climatological composite mean seasonal day, which is constructed by averaging all available days (e.g. for JJA, 92 for each of the single-summer climate model simulations, and 644 for years 2000 to 2006 of the TRMM 3B42 rainfall product). We employ the following diurnal diagnostics:

1. *Harmonic analysis:* For each spatial location, a 24-hour sinusoid is fit to the seasonal composite day time series (transformed to local solar time) to obtain spatial maps of the two degrees of freedom in the curve fit, the phase and amplitude, which are traditionally simultaneously visualized as a vector field (e.g. Wallace 1975). Of course, this technique only provides meaningful information at locations where the sinusoidal curve fit is a reasonable approximation to (i.e. explains a significant fraction of the variance in) the raw mean summer day time series (Dai 2001).
2. *Broadness of the diurnal maximum:* We compute a metric for the broadness, or duration, of the daily maximum in the mean summer day time series of

precipitation. The metric was conceived and is illustrated in Carbone and Tuttle (2008), hereafter CT08. Briefly, it is computed as follows: At each spatial grid point, the time of maximum precipitation in the mean summer day time series is located. Then it is computed how far in time one must march equal distances forward and backward (in time) from the time of maximum precipitation in order to encompass 68 % (i.e. $\pm 1\sigma$) of the total area under the mean summer day precipitation time series. Where the diurnal cycle has an isolated, sharp diurnal maximum this will be a relatively small measure of time whereas for multiply peaked or sinusoidal diurnal cycles it will be a larger measure; hence the CT08 diagnostic is a metric of the broadness of the precipitation maximum in the mean summer day, measured in units of time.

3. *Spatio-temporal variability in the central United States:* Animations of the mean summer day precipitation are constructed using an objective time coordinate (i.e. no transformation to local solar time) to characterize the SP-CAM's ability to simulate sea breeze precipitation and the diurnal propagation of convective precipitation initiated over the Rockies into the central United States.
4. *Reduced transect analysis* Several transects are defined in regions of interest, for detailed regional analysis of the CT08 broadness metric, and the diurnal evolution of parameterized vs. super-parameterized convective heating and moistening.

3. Results

3.1. Harmonic analysis

Figures 2 and 3 show the amplitude and phase of (color hue), and variance attributable to (color saturation), the least squares fitted 24-hour sinusoid, for the DJF and JJA composite days. Figure 2 shows that both models capture the observed tendency for there to be higher diurnal rainfall amplitudes over tropical land masses, tropical convergence zones, and summer hemispheric continents.

The fact that colors are overall unsaturated (i.e. closer to white) for the satellite observations in Figures 2 and 3 indicates that in nature the composite daily cycle of rainfall is not well described by a single sine wave. For CAM, the opposite is true - color hues are uniformly saturated, indicating far too much diurnal variance in the 24-hour mode, a sign that its daily cycle of rainfall is too simple. For the SP-CAM, the results are mixed. In the high amplitude regions of diurnal variability (tropical land masses and tropical ocean convergence zones), decreased color saturation (i.e. increased whiteness) in Figure 2 indicates that the SP-CAM daily cycle of rainfall, like the observations, is more complicated than a simple sine wave. But outside of these most diurnally active parts of the world, for instance over most of the open ocean, the SP-CAM still simulates an overly sinusoidal diurnal rainfall cycle.

In CAM it is clear from Figure 3 that the diurnal cycle is highly consistent over land and ocean respectively, but that these are very different from each other, a property that the observations do not share. The SP-CAM improves in this regard- like the observations there is considerable horizontal inhomogeneity in the phase of the diurnal cycle, both over oceans and within continents. Major documented biases in the amplitude of the 24-hour harmonic in CAM in Figure 2, such as an overly strong diurnal rainfall cycle in the tropics, as well as over South America during JJA, and overly weak diurnal variability over the northwestern tropical Pacific (Collier and Bowman 2004), have been fixed in the SP-CAM.

The seasonal scale wet biases in the SP-CAM manifest themselves as localized excessive 24-hour amplitude maxima in Figure 2. Near the overactive monsoon, Figure 3 shows that the timing of peak precipitation over the Bay of Bengal occurs too early in the SP-CAM, and there is no phase propagation southwest from the Himalayas in the 24-hour mode, which is apparent in the observations. Over the Great Wet Spot bias of the central Pacific, Figure 3 shows that the phase of the 24-hour harmonic is in relatively good agreement with observations, despite excessive amplitude.

Near the United States, Figure 3 also shows that the land-ocean phase inversions associated with the sea breeze diurnal cycle in the Gulf of Mexico and along the eastern seaboard are captured well by the SP-CAM, marking an improvement relative to CAM. Observed phase inversions of the 24-hour mode across the coast of Mexico and western Central America are similarly improved in the SP-CAM. But in the western and central United States, the phase characteristics of the 24-hour mode in the SP-CAM are out of line with observations, and its amplitude is underestimated. The SP-CAM does not capture the observed nocturnal maximum over the continental interior, and the timing of peak precipitation over the Rocky Mountains occurs too early. No eastward phase propagation is evident in the 24-hour mode into the central United States.

3.2. Broadness of the daily maximum

Figure 4 compares the CT08 metric (color hue) of the broadness of the diurnal maximum computed from the climate model simulations against the TRMM 3B42 product, bin-averaged to the models' grid. For the models, the absolute bias in the timing of the precipitation peak is also shown (color saturation). The observations show a clear land-sea contrast in the CT08 metric, with isolated patches of narrower maxima occurring over continental interiors, particularly in the summer hemisphere. The land-sea contrast of the observed CT08 metric is also present in SP-CAM and CAM but in the models these patterns are exaggerated (more so in CAM), with values of the CT08 metric reaching as low as 2 hours (narrow diurnal maxima) over continental interiors (note that diurnal broadness less than the time

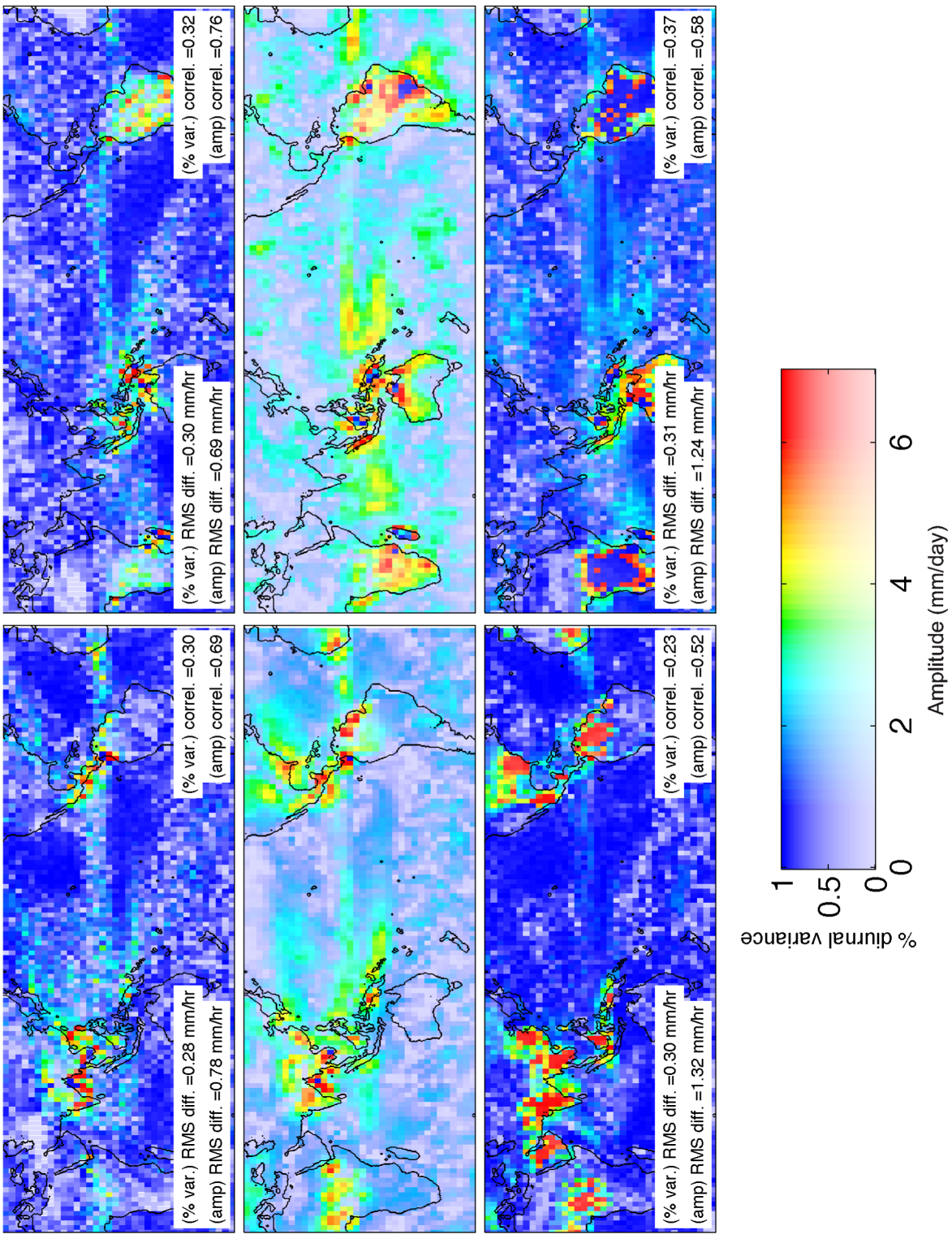

Figure 2. Amplitude of (color hue; mm/day), and variance attributable to (color saturation; fraction) the least squared fitted 24-hour harmonic of precipitation for (top) the SP-CAM, (middle) satellite observations and (bottom) standard CAM, during (left) JJA and (right) DJF. RMS difference and pattern correlation relative to the observations are shown for the two models.

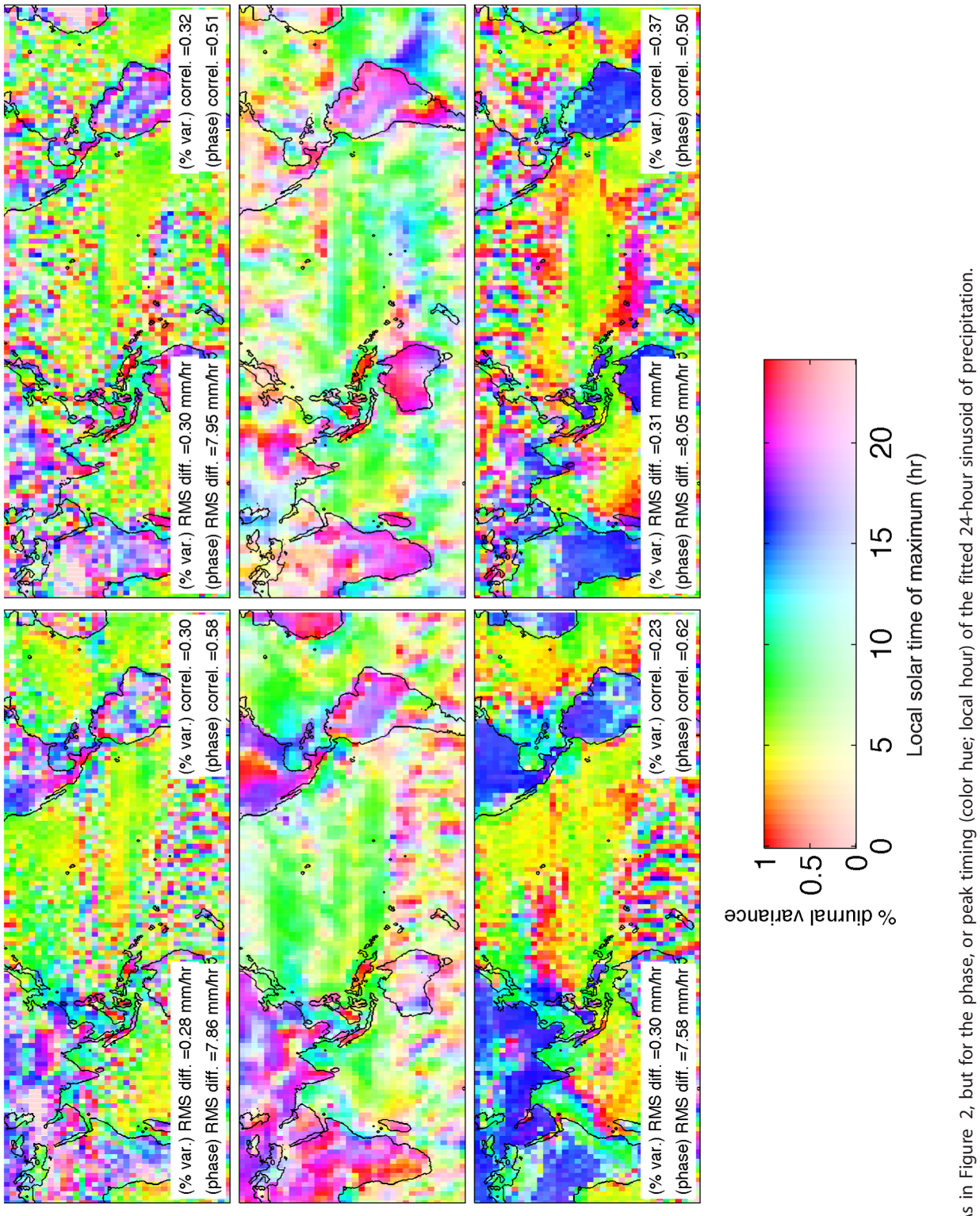

Figure 3. As in Figure 2, but for the phase, or peak timing (color hue; local hour) of the fitted 24-hour sinusoid of precipitation.

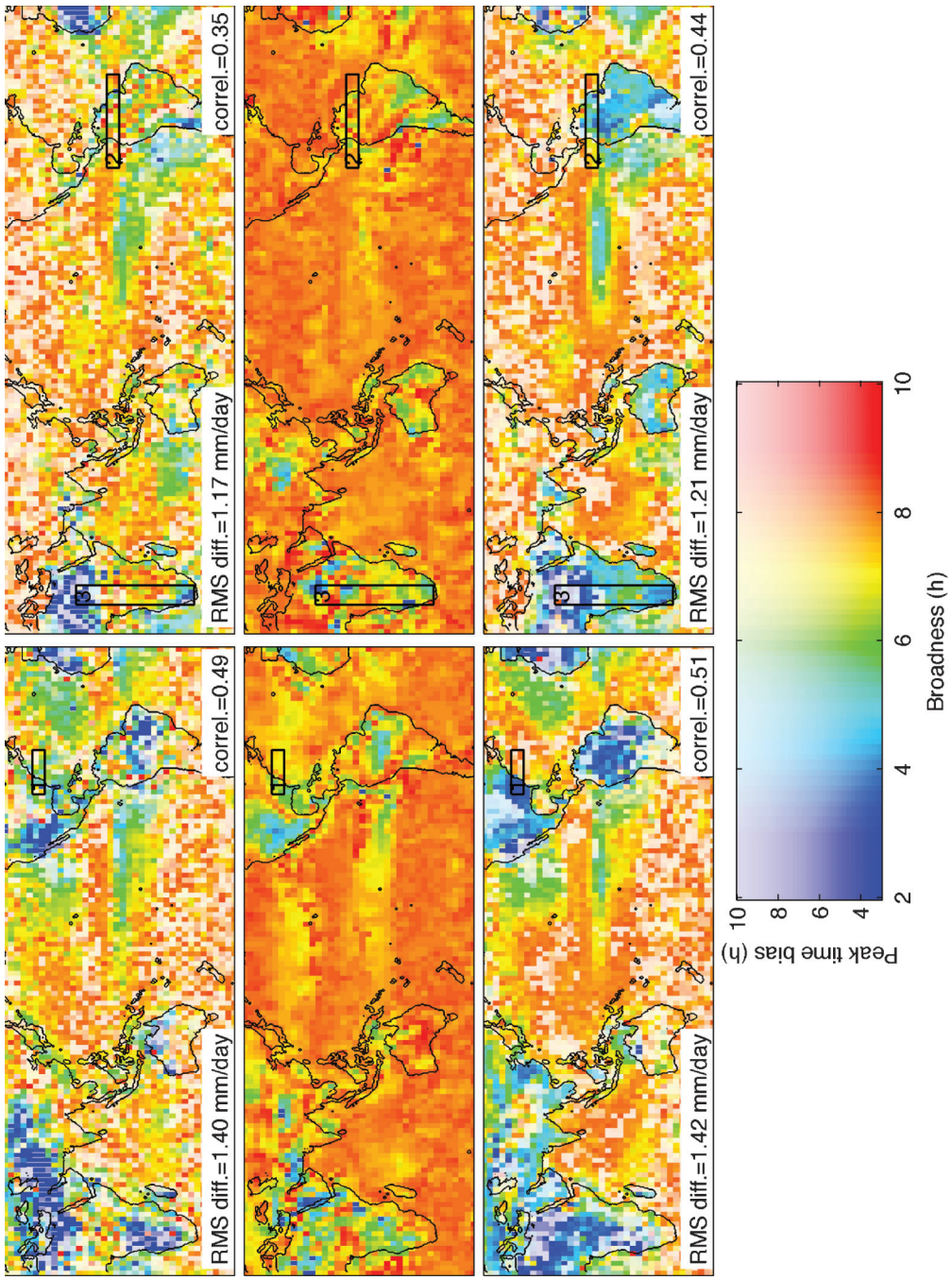

Figure 4. CT08 metric of the broadness of the composite day's precipitation peak (color hue) for (top) the SP-CAM, (middle) satellite observations and (bottom) standard CAM, during (left) JJA and (right) DJF. For the two models, the absolute bias in the time of peak precipitation (color saturation) is also shown. The CT08 broadness quantity is the number of hours that must be marched forward and backward from the time of maximum precipitation in order to encompass 68 % of the total area under the mean summer day precipitation time series. Cool color hues correspond to regions with tightly peaked diurnal cycles, and warm hues correspond to broad or multiply peaked composite diurnal variability.

resolution of the data is possible owing to linear interpolation between the 3-hourly data and output in calculating the CT08 metric). Although such tightly peaked diurnal cycles exist in the full resolution TRMM 3B42 data (not shown), when bin averaged to the model grid the diurnal cycle in the observations is considerably broader than the models in these regions. The observations also show that during boreal summer (JJA), the extratropical coastal ocean bordering eastern Asia and North America exhibits a slightly narrower diurnal peak precipitation than during boreal winter (DJF); this seasonality in the CT08 broadness appears to be captured by the SP-CAM but not by CAM.

Closer inspection of Figure 4 reveals two interesting differences between the structure of the CT08 metric in SP-CAM and CAM. Firstly, within the continental interiors of North America, Africa, and equatorial South America, the broadness of the diurnal cycle in CAM appears to be homogeneously small, in the 2–5 hour range. In contrast, the SP-CAM shows much more horizontal inhomogeneity in the CT08 metric over these land surfaces; there is an east-west contrast over North America, more broadness over equatorial South America, and substantial meridional variability over central Africa. These variations in the SP-CAM's diurnal cycle broadness seem more consistent with the observations, albeit exaggerated in the model in the same fashion as its overall land-sea contrast. Secondly, like the observations, the land-sea contrast of the CT08 metric across coastal ocean boundaries is less sharply defined in the SP-CAM than in CAM.

Is the apparent improvement in the horizontal variability of the precipitation maximum broadness within continents and across coastal boundaries in the SP-CAM a true reflection of improved diurnal cycle variability in these regions, or a coincidence of the way in which the CT08 metric is computed? To find out, we next examine the spatial variability of the seasonal composite day along three transects (shown in Figure 4) where the variability of the CT08 scalar metric of the mean summer day's precipitation in the SP-CAM appears to be improved relative to CAM. For the reasons discussed in Section 2.3, reduced transect analysis is limited to the DJF composite for tropical transects, and to the JJA composite for extratropical transects in the northern hemisphere.

Figure 5 shows that the apparent improvement in the CT08 structure in the SP-CAM along Transect 1 during JJA (zonal transect straddling eastern seaboard and Gulf Stream) is indeed due to an overall improvement in its diurnal cycle of precipitation. The right panels of Figure 5 show the along-transect (zonal) variability in the mean summer day's precipitation in the models and observations, averaged in the cross-transect direction over the transect subdomain. For comparison, the left panels show the variability of the CT08 metric within the same transect subdomain. The along-transect variability in the CAM mean summer day is dominated by an unrealistic strongly peaked diurnal cycle at

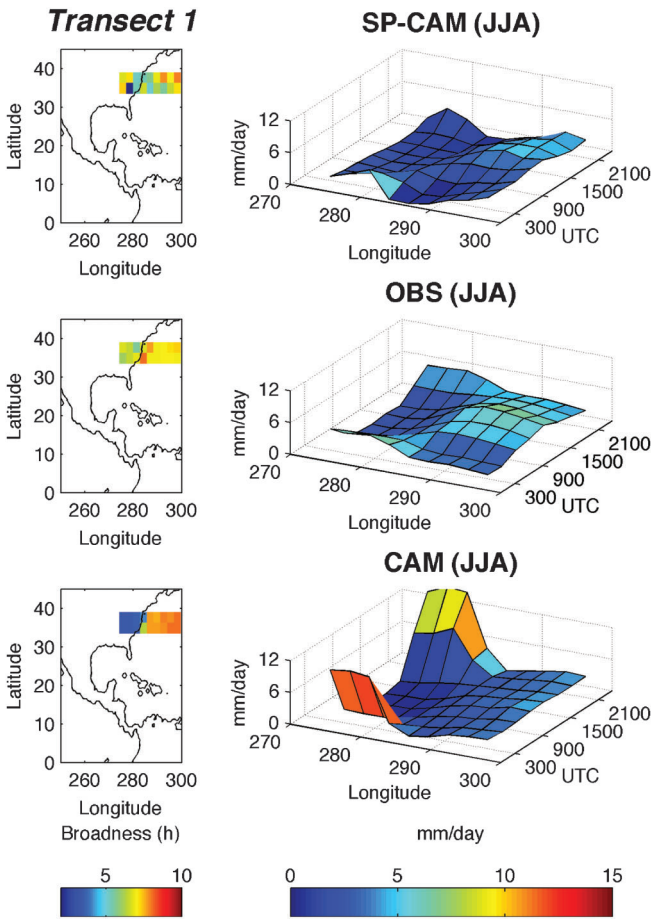

Figure 5. (Left) CT08 metric of the broadness of the mean JJA day's maximum precipitation, shown in a zonal transect domain of interest over the US eastern seaboard and Gulf Stream, comparing the model simulations and the satellite observations, bin-averaged to the model grid. The along-transect structure of the time evolution in the cross-track-averaged mean summer day is shown for comparison to the right.

the west, over land. This is improved in the SP-CAM. Offshore, the opposite occurs. The CAM diurnal cycle of precipitation is too weak over the Gulf Stream portion of the transect, and enhanced in the SP-CAM.

Figure 6 shows that the apparent improvement in the CT08 metric along Transect 2 (zonal DJF transect straddling both coastal boundaries of northern equatorial South America) corresponds to real improvement in the SP-CAM diurnal cycle at the eastern coastal boundary, but not at the west. The right panels of Figure 6 clearly show that CAM has an overly sharp continental peak in the central region of the transect, and does not capture the diurnal cycle phase inversion in the transition from land to sea at the eastern coast; the SP-CAM is improved in these respects. But near the western part of the transect, just interior to the Pacific coast, the SP-CAM diurnal cycle over elevated terrain is much too vigorous, and apparent improvement in the CT08 broadness metric here is misleading.

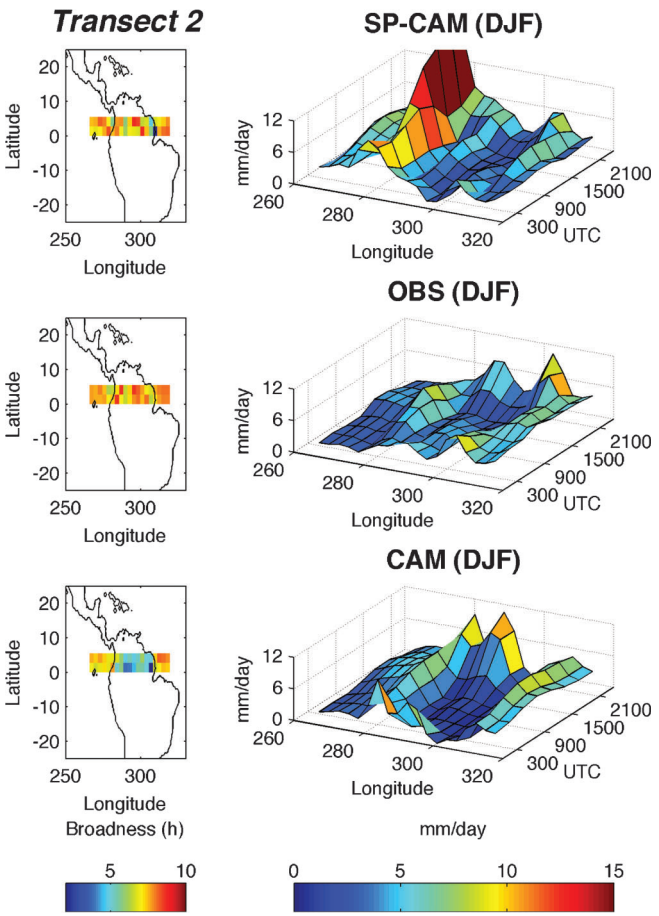

Figure 6. As in Figure 5, but for a DJF zonal transect straddling equatorial South America.

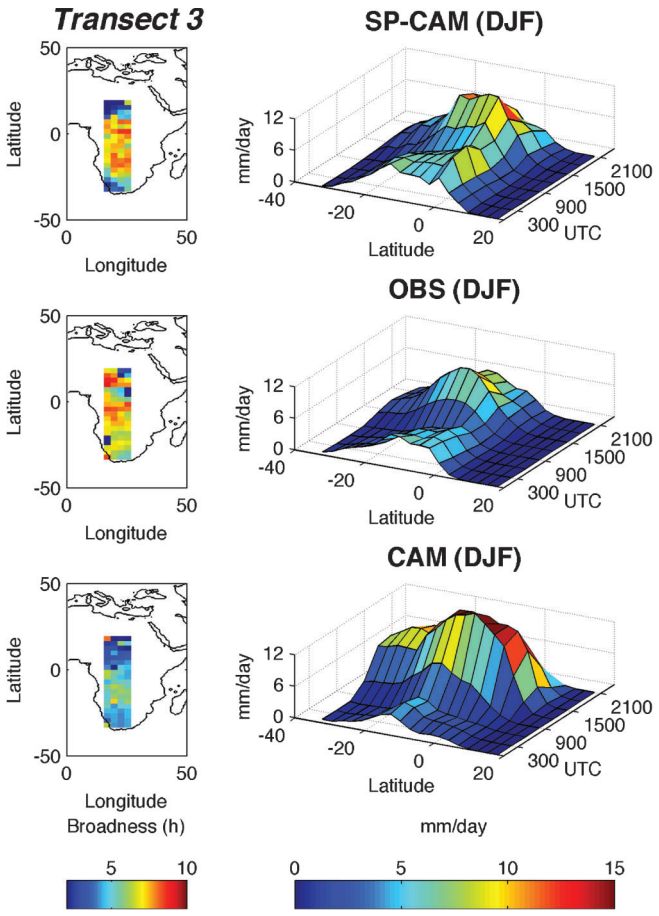

Figure 7. As in Figure 6, but for a DJF meridional transect straddling equatorial Africa.

Finally, Figure 7 shows that apparent improvement in the CT08 metric along Transect 3 (meridional transect through south central Africa) corresponds to real diurnal cycle improvement. In the tropics, the left panels of Figure 7 show that the SP-CAM captures an observed equatorial region of diurnal cycle broadness, while CAM does not. The right panels of Figure 7 show why this is the case; in CAM, the mean summer day over equatorial Africa has a single strong peak near 1500 to 1800 UTC, whereas in the SP-CAM the mean summer day's structure is doubly peaked (0300–0600 UTC, and 1500 UTC) as are the observations (0300–0600 UTC, and 1500 UTC). The first peak occurs earlier (0300 UTC) south of the equator and later (0600 UTC) north of the equator, which is also captured by the SP-CAM, although it overdoes the magnitude of the latter. In the southern portion of Transect 3, only one diurnal peak is observed, whose amplitude decreases with latitude. This feature is also simulated by the SP-CAM; underestimation of CT08 broadness in CAM in the southern part of Transect 3 is again due to overshooting the magnitude of the diurnal peak precipitation over land.

The CT08 metric of the broadness of the mean summer day's precipitation maximum is a difficult diagnostic to interpret, but is a useful tool for identifying features of the diurnal cycle that may not be differentiated via harmonic analysis. In the above analysis, the CT08 diagnostic led us to identify improvements in the SP-CAM's representation of cross-coastal land-sea diurnal cycle variations near the Gulf Stream, improved tropical diurnal variability over equatorial Africa, and improved phasing across the Atlantic coast of north equatorial South America.

3.3. Spatial-temporal variability: North America

Figure 8 and Video S1 [PRECIP.MOV] show the spatial and temporal variability of the composite boreal summer day over North America at the full 3-hourly resolution of the satellite product. This is the most information-rich vantage point from which to evaluate the fidelity of the simulated mean summer day's precipitation. We define the following list of the most significant events in the observations (OBS) as a useful baseline for model comparison:

1. (0600–1500 UTC; Figure 8 c. through f.) A flare of oceanic precipitation occurs over the Gulf Stream current, reaching peak rain rates near 7 mm/day near the midlatitude (offshore) portion of the current

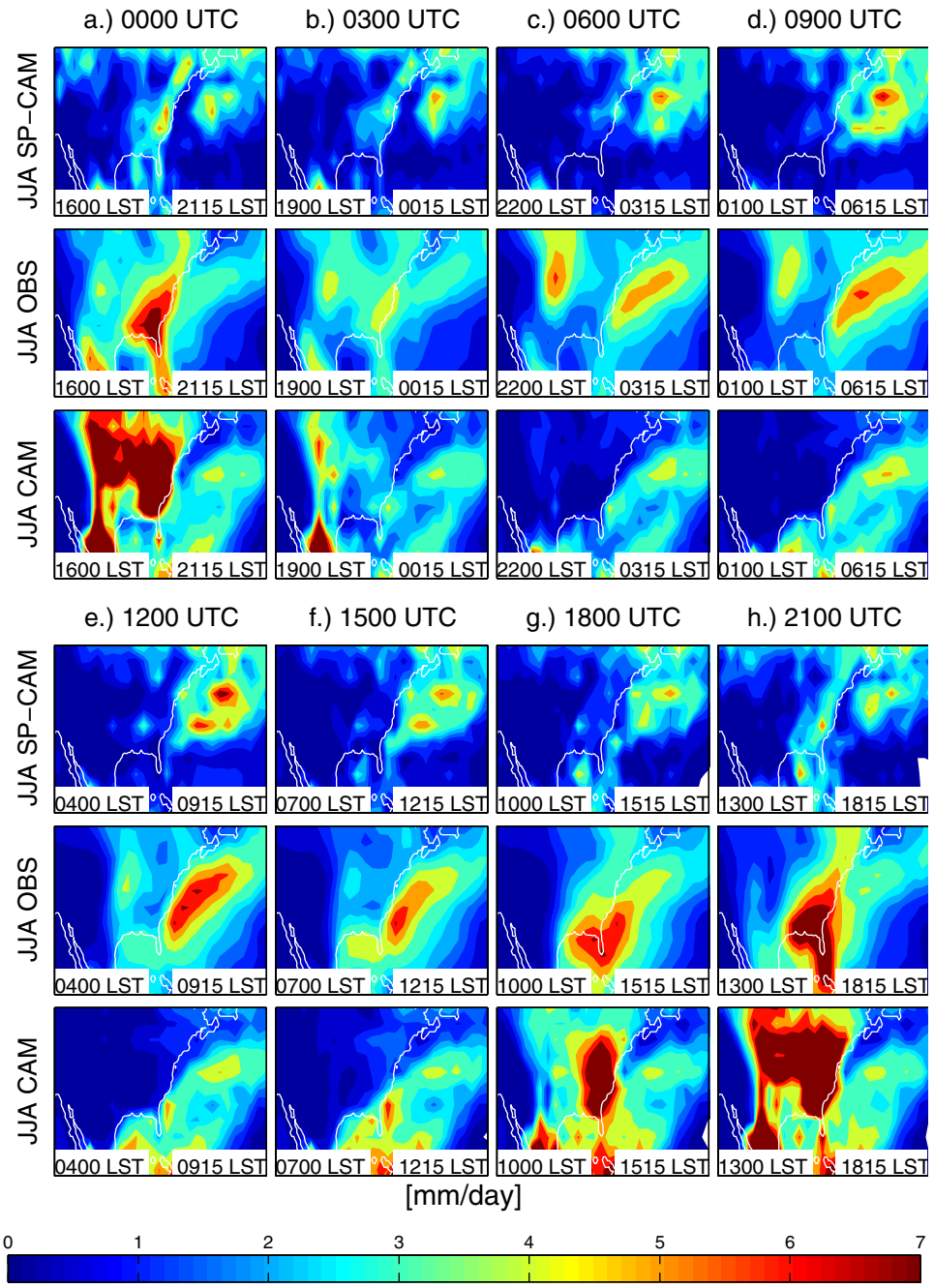

Figure 8. Evolution of the composite JJA day's precipitation over North America, comparing the two climate models against the satellite observations. Snapshots of the 3-hourly average precipitation rate are shown. Local solar time at the longitude axis limits is superimposed at the bottom of each subpanel in text. Note the model-observation-model comparison shown here is more intuitively absorbed in animation format, and we strongly recommend viewing the auxiliary file (PRECIP.mov).

around 1200 UTC (Figure 8 e.), and several hours later for the southern (coastal) portion of the current, peaking around 1500 UTC (Figure 8 f.) off the eastern coast of Florida. From 1200–1800 UTC (Figure 8 e. through g.) there is a southwestward shift in the location and increase in the magnitude of maximum Gulf Stream precipitation in the diurnal composite.

2. (1200–1500 UTC; Figure 8 e. through f.) A localized pulse of offshore precipitation over the coastal ocean borders the northern boundary of the Gulf of Mexico.
3. (1800–0000 UTC; Figure 8 g., h., and a.) The above is followed as it dissipates by a broad pulse of heavy continental precipitation, initiating at the southern extremity of the Florida panhandle where precipitation

rates exceed 7 mm/day over a broad region, and progressing towards the continental interior, with precipitation rates diminishing towards the northwest farther inland.

4. (0000 UTC; Figure 8 a.) A brief pulse of convective precipitation co-located with topographic features in the Western United States, reaching rain rates of 2–3 mm/day.
5. (0300–1200 UTC; Figure 8 b. through e.) Eastward propagation into the central United States of a coherent precipitating feature with rain rates in the 3 mm/day to 5 mm/day range, dissipating as it progresses.

The apparent noisiness in the SP-CAM composite is a result of sporadic, localized precipitation and a relatively short (single summer) composite. When only a single summer of observations is composited (not shown) the result is similarly noisy, although the chronology of events outlined above based on the full 7-summer observation composite is still discernible in each individual summer. The noisiness in the SP-CAM precipitation actually represents an improvement relative to CAM, which within the composite exhibits a too regularly repeated, and expansive, rainfall cycle and thus produces an overly smooth composite from only a single summer of output.

Looking past the noisiness caused by the single season compositing, the SP-CAM does a strikingly better job than CAM at capturing effects (1) through (3) above, but like the CAM it misses (4) and (5). The magnitude and chronology of the diurnal cycle of precipitation over the Gulf Stream (1) are particularly impressive. Here, CAM has little diurnal variability and undiscernable phase differentiation between the phase of the diurnal cycle in the open ocean (northern) segment versus the coastal ocean (southern) portion of the Gulf Stream. With respect to (3), Figure 8 h.,a.,b. reveals that the pattern of southeastern continental precipitation in the SP-CAM from 2100 UTC to 0300 UTC resembles the observations fairly well, although the magnitude is underestimated; there is a fringe of high rainfall adjacent to the east coast (Figure 8 a.), preceded by a localized maximum near Florida (Figure 8 h.). In contrast, Figure 8 h.,a.,b., show that in the CAM mean summer composite day the entire continental interior east of the Rockies experiences a sudden pulse of unrealistically widespread, homogeneous and heavy precipitation, producing high diurnal cycle amplitudes throughout the central United States (as observed) but for the wrong reason (the pattern is incorrect).

Over the continental United States, the satellite data in Figure 8 a. through e. clearly show how a pulse of precipitation initiated over the mountain ranges in the western United States propagates eastward into the continental interior, causing the nocturnal maximum in rainfall. SP-CAM and CAM show markedly different diurnal variability over the continent, with respect to the observations and each other. The top panel of Figure 8 shows that neither model is able to capture the localized afternoon convective precipitation over high topography evident in the observations near 2100 UTC. Thus it is not surprising that subsequent eastward propagation and central United States nocturnal maximum are also not simulated.

4. Discussion

The most energetic locations of diurnal rainfall in the SP-CAM, over tropical land masses and the oceanic convergence zones, are not well fitted with a single 24-hour sine wave, which is an important improvement over CAM. Harmonic analysis shows far too much variance attributable to the 24-hour mode in CAM globally (and in SP-CAM where the diurnal cycle of rainfall is weak) and the CT08 broadness of the CAM diurnal maximum is uniformly too narrow over land surfaces. Transect analysis shows that CAM misses the doubly peaked tropical precipitation cycle over central Africa, favoring sinusoidal variability, and the North American animation shows unrealistically homogeneous pulsating diurnal precipitation over the central United States. In each of the above diagnostics, the SP-CAM diurnal variability, like the observations, appears much less sinusoidal, at least over land masses and in regions of vigorous convection. This can be explained by the fact that in CAM, precipitation is rigidly tied to CAPE which like solar variability varies rather sinusoidally, whereas in the nested cloud resolving subcomponent of the SP-CAM, high resolution moist boundary layer dynamics provide new degrees of freedom for more sophisticated convective activity and moisture transport, which result in a more complex daily rainfall cycle that is not well fit with a single sine wave. The overly sinusoidal weak rainfall cycle in the open ocean remains a perplexing problem in the SP-CAM.

The SP-CAM approach does not admit diurnally propagating orogenic precipitation systems over the Central United States, which explains the model's seasonal scale dry bias in this region. We suspect the SP-CAM fails to resolve orogenic propagating organized precipitation due to two key design limitations:

1. *Topographic convective heating* is suppressed on the cloud-resolving subdomain scale in the SP-CAM. In nature, propagating meso-scale organization is initiated by a pulse of afternoon convection over the Rockies that is in part due to the efficient warming of steeply sloped topography during the morning hours. However in the SP-CAM, radiative calculations on the cloud-resolving subdomain assume uniform topographic gradients colocated with the spectrally smoothed topography of the coarse-resolution host GCM. The consequent lack of strong afternoon mountain heating in the SP-CAM distorts the structure of the lowlevel wind circulation in the lee of the Rockies (not shown); diurnally propagating organized convection depends upon this background circulation to deliver nocturnal CAPE, and to propagate (Moncrieff and Liu 2006).

2. *The use of periodic boundary conditions* in the cloud-resolving subdomain: Although necessary from a technical and parallel computing perspective, the fact that CRM columns don't communicate across host GCM grid cell boundaries in the SP-CAM limits the ability for propagation of organized convection to the extent that it can be mediated via its influence on large scale motions. Although this is apparently not an obstacle for the propagation of the MJO, it likely limits the degree to which smaller-scale organized convection can propagate and sustain itself in the SP-CAM, especially at T42 spectral resolution in the host GCM.

4.1. Coastal diurnal rainfall in the SP-CAM

The SP-CAM appears to do a better job at capturing structural changes in the diurnal cycle of precipitation across land-sea boundaries. The North American animations also show that the SP-CAM has improved the overall progression of precipitation events over the Gulf Stream, Gulf of Mexico and southeastern continental United States, as well as the diurnal variation of lower tropospheric winds over the moist southern portion of the nocturnal low-level jet (not shown). The cross-coastal contrast in the broadness of the diurnal cycle maximum is smaller in the SP-CAM than in CAM, and transect analysis shows that this is due to improved representation of shifts in diurnal rainfall cycle across coastal boundaries.

Figure 9 explores the coastal diurnal cycle improvement in the SP-CAM by contrasting the vertical and along-transect diurnal evolution of heating and moistening due to convection in the two models, along the Gulf Stream zonal transect discussed previously. In the case of the CAM3, these convective tendencies are diagnosed in the model physics package by the Zhang-McFarlane and Hack convection schemes (model variables ZMDT, ZMDQ, CMFDQ, CMFDT). In the case of SP-CAM, all the sub-grid-scale tendencies that include cloud processes but exclude radiative heating rates are computed by the embedded CRMs; details are given by Khairoutdinov et al. (2005). In Figure 9 the most thermodynamically significant difference between the two models' diurnal cycle is the daytime convective heating and moistening (in the SP-CAM) of the lower and mid troposphere over land. In the western part of the transect, from 0630 to 0930 LST (9 e.,f.) vertically confined convection in the SP-CAM manifests as a shallow layer of convective heating near the surface. Above the deepening SP-CAM boundary layer the mid-troposphere is cooled and moistened by the influence of the nested CRM. This suggests entrainment mixing by shallow convection is playing a role, as is captured by CRMs run in full three dimensional domains (Guichard et al. 2004, Bretherton 2007). Likewise, preconditioning of the mid troposphere is likely responsible for delaying the onset of subsequent deep convection over land in the SP-CAM, resulting in the improved diurnal timing of peak diurnal rainfall, and also drastically altering the chronology and vertical structure of thermodynamic forcing on the atmospheric column adjacent to the ocean, relative to CAM. The same coastal land inter-model difference shown in Figure 9 can be seen in many other cross-coastal transects, straddling the Maritime Continent, equatorial South America, and the Gulf of Mexico (not shown). For the Gulf Stream transect, we have also verified that this over-land chronology in the composite is regularly repeated on a day-to-day basis.

Over the oceanic (eastern) portion of the transect, Figure 9 shows that CAM tends to convect deeply at all times of day, presumably because its formulation of deep convection is cast in terms of undilute CAPE and thus constantly triggered by the high surface fluxes over the Gulf Stream. In the SP-CAM, most of the enhanced day-to-day variability over the Gulf Stream occurs in a shallow convective boundary layer which deepens and invigorates nocturnally (Figure 9a.–c.), apparently following humidification (cooling and moistening) of air atop a very thin convective layer during the day (Figure 9 f.–h.). Unlike the SP-CAM diurnal chronology of convective heating higher up in the atmosphere discussed below, this boundary layer cycle over the Gulf Stream in the SP-CAM occurs regularly on individual days. Further evidence that low cloud processes are involved in the enhanced SP-CAM diurnal rainfall cycle is provided by the fact peak Gulf Stream rainfall coincides with a southward extension of a broader area of high low-cloud fraction in the North Atlantic (not shown). In fact, all climatological regions of low cloud coverage exhibit more areal diurnal expansion and contraction in the SP-CAM than in the CAM (not shown).

In Figure 9 c.–f., the apparent eastward propagation of a mid-tropospheric convective heating signal in the SP-CAM diurnal composite near $\sigma = 0.5$ is difficult to interpret because it appears sporadically on individual days. We hesitate to attribute this signal as a dynamical connection between the land thermal oscillator and the ocean diurnal cycle, as was noted for instance in the mesoscale simulation of Mapes et al. (2003)), due to the possibility that this signal may be caused by aliasing of eastward propagating synoptic events into a relatively noisy single-season diurnal composite. However the possibility of a free atmospheric wave mechanism linking land and coastal ocean diurnal cycles in the SP-CAM is intriguing. Although the gravity wave process implicated in the tropical study of Mapes et al. (2003) is unlikely to be resolvable by the SP-CAM (since adjacent gravity-wave-resolving CRMs cannot propagate information across host model grid boundaries), larger-scale mechanisms active in midlatitudes, such as inertia-gravity waves, or synoptic advection of convective heating anomalies induced by the embedded CRM, could be operative in linking Gulf Stream diurnal precipitation with thermal forcing over land in the SP-CAM. This merits further investigation.

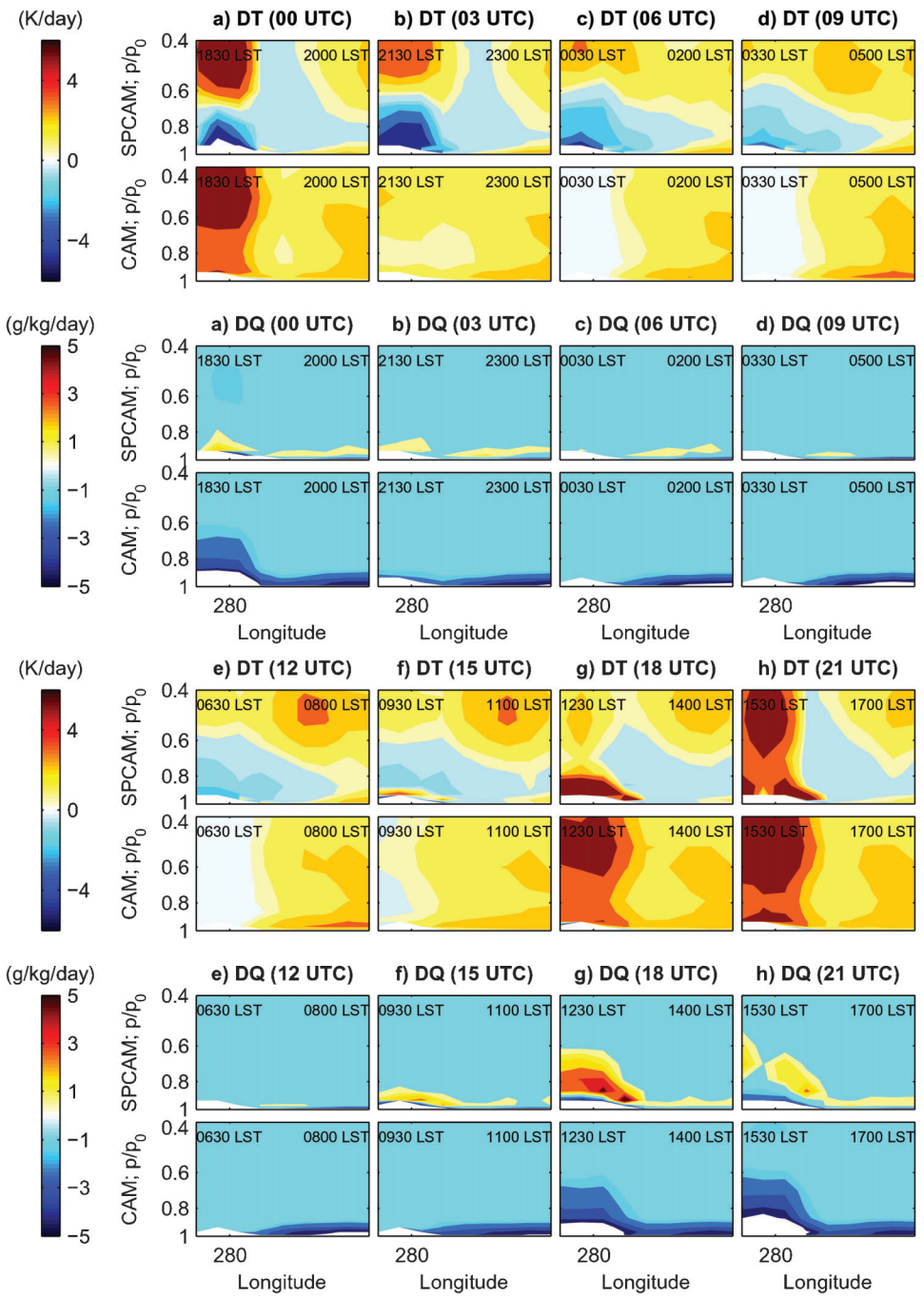

Figure 9. Height-longitude section contrasting the diurnal chronology of convective heating and convective moistening in the SP-CAM and the CAM, along a zonal transect straddling the Gulf Stream and eastern United States (Transect 1 in Figure 4). The quantities shown are tendencies exerted by convection in the physics package, i.e. by nudging towards the nested CRM in the SP-CAM and as diagnosed by conventional parameterization in CAM. The vertical coordinate is normalized pressure ($\sigma = p/1000$ hPa), and the land component at the western edge of the transect is identifiable as a blanked out region at the base of the domain. As in figure 8 strongly recommend viewing the auxiliary animation file (CONVTEND.mov).

5. Conclusions

We have combined multiple, complementary diagnostics of the seasonal composite diurnal cycle of surface precipitation in order to characterize the performance of moist dynamics in a multi-scale modeling framework (SP-CAM) and its GCM counterpart (CAM) on these timescales, using satellite data as a baseline for model evaluation. Each diurnal cycle diagnostic comes with pros and cons. Traditional harmonic analysis allows an analysis of the global structure of both the

strength and phase of sinusoidal diurnal cycles, but is only applicable to regions where this curve fit is a reasonable approximation. The non-traditional CT08 metric of the broadness of the peak precipitation distinguishes narrowly peaked diurnal cycles from broader, or doubly peaked diurnal cycles, without the necessity for curve fitting, but there is a degeneracy problem in that very different diurnal cycles can produce the same result. Animations or reduced dimension transects of the full spatial and temporal variability of the climatological seasonal composite day provide the most information-rich perspective for model evaluation, but must be undertaken regionally and are difficult to summarize since their interpretation can be subjective.

Combining all of these perspectives, several common features distinguishing the diurnal rainfall cycle in the SP-CAM from CAM may be summarized. Positive features in SP-CAM include:

- Less sinusoidal variability where diurnal rainfall is vigorous,
- Less overestimation of diurnal rainfall over tropical and summer hemispheric land masses,
- Good representation of the observed structural transitions of diurnal rainfall across coastal ocean boundaries.
- More horizontal inhomogeneity of diurnal rainfall cycles within continents and within oceans,
- Improved chronology of diurnal precipitation in the southeastern United States, western Atlantic and Gulf of Mexico diurnal composite.

Remaining negative features of the SP-CAM diurnal rainfall cycle include:

- No orogenic propagating precipitation over the central United States.
- Excessive diurnal variability associated with the overactive monsoon
- Overly sinusoidal diurnal rainfall over most of the open ocean

Follow up regional sensitivity studies are recommended to tease out the mechanisms involved in regulating the coastal ocean diurnal precipitation and the mechanisms that may link it to the improved representation of convective heating and moistening over adjacent land in the SP-CAM. Also, since precipitation is only one component of the hydrologic budget, analysis of the complementary diurnal variations of evaporation, moisture storage, and moisture flux convergence, as in Randall et al. (1991), would complement this work by providing a more complete picture of the physical processes underlying diurnal moist dynamics in the SP-CAM.

Acknowledgments: We are grateful to the late John Roads, and to David Randall, Guang Zhang, Joel Norris, Mitch Moncrieff, Gabe Kooperman, Gregory Elliassen, Kate Thayer-Calder, and John Helly for insightful conversations about this work. We are especially indebted to Curtis Covey and an anonymous reviewer for highly constructive feedback. This research was supported by the Center for Multiscale Modeling of Atmospheric Processes (CMMAP), an NSF Science and Technology Center managed by Colorado State University under cooperative agreement No. ATM-0425247. Computing resources were provided by NSF TeraGrid (TG-ATM080014T and TG-ATM080011T) consumed at the San Diego Supercomputing Center and at Purdue.

References

Bretherton, C. S., 2007: Challenges in numerical modeling of tropical circulations. In *The Global Circulation of the Atmosphere*, T. Schneider and A. H. Sobel, Eds., Princeton University Press, 302–330.

Carbone, R. E. and J. D. Tuttle, 2008: Rainfall occurrence in the United States warm season: The diurnal cycle. *Journal of Climate*, **21** (16), 4132–4146, doi: 10.1175/2008JCLI2275.1.

Carbone, R. E., J. D. Tuttle, D. Ahijevych, and S. B. Trier, 2002: Inferences of predictability associated with warm season precipitation episodes. *Journal of the Atmospheric Sciences*, **59**, 2033–2056, doi: 10.1175/1520-0469(2002)059<2033:IOPAWW>2.0.CO;2.

Chang, A., L. Chiu, and G. Yang, 1995: Diurnal cycle of oceanic precipitation from SS/MI data. *Monthly Weather Review*, **123** (11), 3371–3380, doi: 10.1175/1520-0493(1995)123<3371:DCOOPF>2.0.CO;2.

Collier, J. C. and K. P. Bowman, 2004: Diurnal cycle of tropical precipitation in a general circulation model. *Journal of Geophysical Research - Atmospheres*, **109** (D17), doi: 10.1029/2004JD004818.

Collins, W., P. Rasch, B. Boville, J. Hack, J. McCaa, D. Williamson, B. Briegleb, C. Bitz, S. Lin, and M. Zhang, 2006: The formulation and atmospheric simulation of the Community Atmosphere Model version 3 (CAM3). *Journal of Climate*, **19** (11), 2144–2161, doi: 10.1175/JCLI3760.1.

Dai, A. G., 2001: Global precipitation and thunderstorm frequencies. Part II: Diurnal variations. *Journal of Climate*, **14**, 1112–1128, doi: 10.1175/1520-0442(2001)014<1112:GPATFP>2.0.CO;2.

Dai, A. G., X. Lin, and K. L. Hsu, 2007: The frequency, intensity, and diurnal cycle of precipitation in surface and satellite observations over low- and mid-latitudes. *Climate Dynamics*, **29** (7–8), 727–744, doi: 10.1007/s00382-007-0260-y.

DeMott, C. A., D. A. Randall, and M. Khairoutdinov, 2007: Convective precipitation variability as a tool for general circulation model analysis. *Journal of Climate*, **20** (1), 91–1121, doi: 10.1175/JCLI3991.1.

Grabowski, W. W. and P. K. Smolarkiewicz, 1999: CRCP: a cloud resolving convective parameterization for modeling the tropical convective atmosphere. *Physica D*, **133**, 171–178, doi: 10.1016/S0167-2789(99)00104-9.

Guichard, F., J. C. Petch, J. L. Redelsperger, P. Bechtold, J. P. Chaboureau, S. Cheinet, W. Grabowski, H. Grenier, C. G. Jones, M. Kohler, J. M. Piriou, R. Tailleux and

M. Tomasini, 2004: Modelling the diurnal cycle of deep precipitating convection over land with cloud-resolving models and single-column models. *Quarterly Journal of the Royal Meteorological Society*, **130** (604), 3139–3172, doi: 10.1256/qj.03.145.

Hirose, M., R. Oki, S. Shimizu, M. Kachi, and T. Higashiuwatoko, 2008: Finescale diurnal rainfall statistics refined from eight years of TRMM PR data. *Journal of Applied Meteorology and Climatology*, **47** (2), 544–5611, doi: 10.1175/2007JAMC1559.1.

Huffman, G., R. Adler, D. Bolvin, G. Gu, E. Nelkin, K. Bowman, Y. Hong, E. Stocker, and D. Wolff, 2007: The TRMM multisatellite precipitation analysis (TMPA): Quasi-global, multiyear, combined-sensor precipitation estimates at fine scales. *Journal of Hydrometeorology*, **8** (1), 38–55, doi: 10.1175/JHM560.1.

Khairoutdinov, M., C. DeMott, and D. Randall, 2008: Evaluation of the simulated interannual and subseasonal variability in an AMIP-style simulation using the CSU multi-scale modeling framework. *Journal of Climate*, **21** (3), 413–431, doi: 10.1175/2007JCLI1630.1.

Khairoutdinov, M., D. Randall, and C. DeMott, 2005: Simulations of the atmospheric general circulation using a cloud-resolving model as a superparameterization of physical processes. *Journal of the Atmospheric Sciences*, **62** (7), 2136–2154, doi: 10.1175/JAS3453.1.

Khairoutdinov, M. F. and D. A. Randall, 2003: Cloud resolving modeling of the ARM summer 1997 IOP: Model formulation, results, uncertainties, and sensitivities. *Journal of the Atmospheric Sciences*, **60** (4), 607–625, doi: 10.1175/1520-0469(2003)060<0607:CRMOTA>2.0.CO;2.

Kikuchi, K. and B. Wang, 2008: Diurnal precipitation regimes in the global tropics. *Journal of Climate*, **21** (11), 2680–2696, doi: 10.1175/2007JCLI2051.1.

Luo, Z. Z. and G. L. Stephens, 2006: An enhanced convection-wind-evaporation feedback in a superparameterization GCM (SP-GCM) depiction of the Asian summer monsoon. *Geophysical Research Letters*, **33** (6), Art. No. L06 707, doi: 10.1029/2005GL025060.

Mapes, B. E., T. T. Warner and M. Xu, 2003: Diurnal patterns of rainfall in northwestern South America. Part III: Diurnal gravity waves and nocturnal convection offshore. *Monthly Weather Review*, **5** (131), 830–844, doi: 10.1175/1520-0493(2003)131<0830:DPORIN>2.0.CO;2.

Moncrieff, M. W. and C. H. Liu, 2006: Representing convective organization in prediction models by a hybrid strategy. *Journal of the Atmospheric Sciences*, **63** (12), 3404–3420, doi: 10.1175/JAS3812.1.

Pritchard, M. S. and R. C. J. Somerville, 2009: Empirical orthogonal function analysis of the diurnal cycle of precipitation in a multi-scale climate model. *Geophysical Research Letters*, **36** (L05812), doi: 10.1029/2008GL036964.

Randall, D., M. Khairoutdinov, A. Arakawa, and W. Grabowski, 2003: Breaking the cloud parameterization deadlock. *Bulletin of the American Meteorological Society*, **84** (11), 1547–1562, doi: 10.1175/BAMS-84-11-1547.

Randall, D. A., Hashvardhan, and D. A. Dazlich, 1991: Diurnal variability of the hydrologic-cycle in a general-circulation model. *Journal of the Atmospheric Sciences*, **48** (1), 40–62, doi: 10.1175/1520-0469(1991)048<0040:DVOTHC>2.0.CO;2.

Tao, W.-K., J.-D. Chern, R. Atlas, D. Randall, M. Khairoutdinov, J.-L. Li, D. E. Waliser, A. Hou, X. Lin, C. Peters-Lidard, W. Lau, J. Jian, and J. Simpson, 2009: A multiscale modeling system - Developments, applications, and critical issues. *Bulletin of the American Meteorological Society*, **90** (4), 515–534, doi: 10.1175/2008BAMS2542.1.

Wallace, J. M., 1975: Diurnal-variations in precipitation and thunderstorm frequency over conterminus United States. *Monthly Weather Review*, **103** (5), 406–419, doi: 10.1175/1520-0493(1975)103<0406:DVIPAT>2.0.CO;2.

Zhang, Y., S. A. Klein, C. Liu, B. Tian, R. T. Marchand, J. M. Haynes, R. B. McCoy, Y. Zhang, and T. P. Ackerman, 2008: On the diurnal cycle of deep convection, high-level cloud, upper troposphere water vapor in the Multiscale Modeling Framework. *Journal of Geophysical Research – Atmospheres*, **113** (D16105), doi: 10.1029/2008JD009905.